Arginine-deprivation–induced oxidative damage sterilizes *Mycobacterium tuberculosis*

Sangeeta Tiwari[a,1], Andries J. van Tonder[b], Catherine Vilchèze[a,c], Vitor Mendes[d], Sherine E. Thomas[d], Adel Malek[a], Bing Chen[a], Mei Chen[a], John Kim[a], Tom L. Blundell[d], Julian Parkhill[b], Brian Weinrick[a], Michael Berney[a], and William R. Jacobs Jr.[a,c,1]

[a]Department of Microbiology and Immunology, Albert Einstein College of Medicine, Bronx, NY 10461; [b]Wellcome Sanger Institute, Wellcome Genome Campus, Hinxton, Cambridge, CB10 1SA, United Kingdom; [c]Howard Hughes Medical Institute, Albert Einstein College of Medicine, Bronx, NY 10461; and [d]Department of Biochemistry, University of Cambridge, Cambridge, CB2 1GA, United Kingdom

Contributed by William R. Jacobs Jr., July 17, 2018 (sent for review June 1, 2018; reviewed by Peter Belenky and James J. Collins)

Reactive oxygen species (ROS)-mediated oxidative stress and DNA damage have recently been recognized as contributing to the efficacy of most bactericidal antibiotics, irrespective of their primary macromolecular targets. Inhibitors of targets involved in both combating oxidative stress as well as being required for in vivo survival may exhibit powerful synergistic action. This study demonstrates that the de novo arginine biosynthetic pathway in *Mycobacterium tuberculosis* (*Mtb*) is up-regulated in the early response to the oxidative stress-elevating agent isoniazid or vitamin C. Arginine deprivation rapidly sterilizes the *Mtb* de novo arginine biosynthesis pathway mutants Δ*argB* and Δ*argF* without the emergence of suppressor mutants in vitro as well as in vivo. Transcriptomic and flow cytometry studies of arginine-deprived *Mtb* have indicated accumulation of ROS and extensive DNA damage. Metabolomics studies following arginine deprivation have revealed that these cells experienced depletion of antioxidant thiols and accumulation of the upstream metabolite substrate of ArgB or ArgF enzymes. Δ*argB* and Δ*argF* were unable to scavenge host arginine and were quickly cleared from both immunocompetent and immunocompromised mice. In summary, our investigation revealed in vivo essentiality of the de novo arginine biosynthesis pathway for *Mtb* and a promising drug target space for combating tuberculosis.

L-arginine | reactive oxygen species | oxidative damage | *Mycobacterium tuberculosis* | bactericidal auxotrophy

Tuberculosis (TB), caused by *Mycobacterium tuberculosis* (*Mtb*), is a global health problem that causes 1.7 million deaths each year. Long chemotherapy, misdiagnosis, and emergence of multidrug-resistant strains mandate the need to identify novel vulnerable *Mtb* metabolic pathways to develop more efficient drugs to shorten chemotherapy (1). Moreover, systematic understanding of the adaptive mechanisms used by *Mtb* to develop resistance to the existing mycobactericidals will help to identify novel therapeutic approaches to prevent sensitive bacteria from developing resistance during treatment (2).

Presently, in both Gram-positive and Gram-negative bacteria, the role of reactive oxygen species (ROS) generated by metabolic perturbations leading to oxidative damage is well understood. Most of the bactericidal antibiotics that target *Escherichia coli* induce lethality by a common mechanism despite having different primary targets (3–7). This common response involves changes in iron and redox metabolism and accumulation of ROS causing oxidative damage of DNA, RNA, and proteins, ending in cell death (7). ROS-mediated oxidative damage is also a recognized rapid killing mechanism for *Mtb* (8–13). The mycobactericidals isoniazid (INH) and vitamin C have been shown to induce rapid death of *Mtb* by ROS generation, leading to oxidative damage (8, 9, 13). Nonetheless, early adaptive responses of *Mtb* to INH- and vitamin C-induced ROS have yet to be characterized.

Through transcriptional profiling, this study identifies the de novo arginine biosynthesis pathway as one of the early adaptive responses of *Mtb* to oxidative stress promoting mycobactericidals vitamin C and INH. Since other studies in cancer cells, *Burkholderia cenocepacia*, and *Leishmania donovani* have shown that arginine deprivation leads to ROS generation, oxidative damage, and cell death (14–17), we have further investigated the effect of arginine deprivation in *Mtb*. Using an integrated approach of genetics, transcriptomics, flow cytometry-based analysis, metabolomics, and animal models, our study demonstrates the absolute essentiality of the de novo arginine biosynthesis pathway for *Mtb* in the absence of pathway intermediates or exogenous arginine. Disruption of the de novo arginine biosynthesis pathway leads to depletion of antioxidant thiols, accumulation of upstream metabolite substrates of the deleted enzymes (ArgB or ArgF) in the arginine biosynthetic pathway, followed by ROS-mediated oxidative damage and rapid sterilization of *Mtb* populations both in vitro and in vivo.

Results

Arginine Deprivation of *Mtb* Leads to Rapid Sterilization. Previous studies have shown that INH and vitamin C kill *Mtb* in part by inducing oxidative damage (8, 9). Therefore, to identify *Mtb*'s initial transcriptional signatures as an adaptive response to these mycobactericidals, we performed RNA-Seq on *Mtb* cultures both untreated and treated with INH (1 μg/mL) or vitamin C (4 mM) for

Significance

Tuberculosis results in over 1.7 million deaths annually; this problem is worsened by the emergence of drug-resistant strains. New drugs and a better understanding of the mechanisms of existing interventions are needed to prevent the development of drug resistance. Reactive oxygen species (ROS)-mediated lethality by bactericidal drugs was observed in *Mycobacterium tuberculosis* (*Mtb*). Our studies demonstrate that arginine deprivation sterilizes for *Mtb* in vitro and in the host. Using several complementary approaches, we show that arginine deprivation leads to the depletion of thiols, accumulation of ROS, DNA damage, and rapid *Mtb* death. We propose enzymes in the de novo arginine biosynthesis pathway represent promising drug target candidates to be inhibited to treat *Mtb* and its drug-resistant strains.

Author contributions: S.T. and W.R.J. designed research; S.T., A.J.v.T., C.V., V.M., S.E.T., B.C., M.C., J.K., and B.W. performed research; T.L.B. and J.P. contributed new reagents/analytic tools; S.T., A.J.v.T., C.V., V.M., S.E.T., A.M., B.C., M.C., J.K., T.L.B., J.P., B.W., M.B., and W.R.J. analyzed data; and S.T. and W.R.J. wrote the paper.

Reviewers: P.B., Brown University; and J.J.C., Massachusetts Institute of Technology.

The authors declare no conflict of interest.

Data deposition: The microarray raw data have been deposited in the Gene Expression Omnibus (GEO) database at https://www.ncbi.nlm.nih.gov/geo (accession no. GSE98821).

See Commentary on page 9658.

[1]To whom correspondence may be addressed. Email: sangeeta.tiwari@einstein.yu.edu or jacobsw@hhmi.org.

This article contains supporting information online at www.pnas.org/lookup/suppl/doi:10.1073/pnas.1808874115/-/DCSupplemental.

Published online August 24, 2018.

4 h. Of the six genes up-regulated in response to both of the treatments, four (*argB*, *argC*, *argD*, *argJ*) are involved in the de novo arginine biosynthesis (Fig. 1*A*). This result suggests a role for the arginine biosynthesis pathway in tolerating oxidative stress generated by these bactericidal agents. This prompted us to investigate the role of this pathway in *Mtb* survival. The biosynthetic pathway for de novo biosynthesis of L-arginine in *Mtb* consists of eight catalytic steps performed by eight enzymes encoded by the genes *argA*, *argB–D*, *argF–H*, and *argJ*. Using bioinformatics approaches and the results of genetic screens (18), we determined that the gene *argB*, which encodes an acetylglutamate kinase and the second enzyme in the pathway (*SI Appendix*, Fig. S1*A*), is essential to *Mtb* and lacks a human homolog, thus fulfilling key drug-target criteria. Ornithine carbamoyltransferase, encoded by *argF*, was additionally chosen for study as it produces the important nonproteinogenic amino acid citrulline (*SI Appendix*, Fig. S1*A*). Δ*argB* and Δ*argF* mutants, generated using specialized transduction in the clinical isolate CDC1551 and in the laboratory strain H37Rv of *Mtb* (*SI Appendix*, Tables S1–S3), were confirmed by PCR (*SI Appendix*, Fig. S1*B*). Neither mutant grew in unsupplemented media (*SI Appendix*, Fig. S1 *C* and *D*), but growth was restored completely by the addition of 0.5–1 mM L-arginine or by genetic complementation (*SI Appendix*, Fig. S1 *C–E* and Tables S1 and S2). Supplementation with the arginine pathway intermediates L-ornithine or L-citrulline restored Δ*argB* growth in the absence of L-arginine (*SI Appendix*, Fig. S2*A*). We further tested whether arginine starvation is bactericidal or bacteriostatic for *Mtb* CDC1551. Arginine deprivation remarkably caused a greater than 4-log decrease in Δ*argB* and Δ*argF* colony-forming units (cfu) within day 10, whereas when other auxotrophs were deprived of their respective nutrients, the effect was bacteriostasis (Δ*leuCD*, leucine; Δ*panCD*, pantothenate) or a more limited ∼3-log decrease for a bactericidal auxotrophy (Δ*metA*, methionine) (*SI Appendix*, Fig. S2*B*). The rapid killing of Δ*argB* and Δ*argF* was independent of strain background, as we observed the same rapid death with Δ*argB* and Δ*argF* mutants of H37Rv; no cfu were isolated for Δ*argB*, indicating complete sterilization by day 20 or 40, depending on the initial number of *Mtb* cells used, 10^6 or 10^7 cfu/mL, respectively (Fig. 1*B* and *SI Appendix*, Fig. S2*C*). Similarly, no cfu were isolated for Δ*argF* after day 40 of the arginine starvation (Fig. 1*C*). Addition of exogenous L-arginine to the arginine-deprived cultures at day 40 was unable to rescue the Δ*argB* mutant (*SI Appendix*, Fig. S2*D*), suggesting a lack of persistent viable cell populations to resume growth. No suppressor mutants were isolated after plating 10^9 cells of Δ*argB* or Δ*argF* in three independent experiments. Thus, using two independent mutants in the de novo arginine biosynthetic pathway, we found that arginine deprivation leads to rapid sterilization of Δ*argB* and Δ*argF* in vitro without the emergence of suppressor mutants.

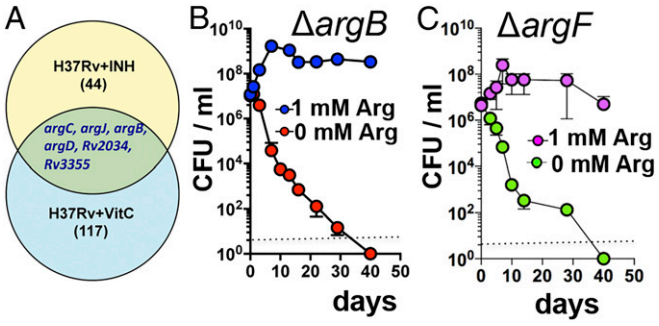

Fig. 1. Deprivation of L-arginine sterilizes pathogenic *Mtb*. (*A*) Venn diagram showing up-regulation of de novo arginine biosynthesis in *Mtb* cells treated with 1 μg/mL INH or 4 mM vitamin C (Vit C) for 4 h. Starvation-death response of *Mtb* Δ*argB* (*B*) and Δ*argF* (*C*) ±1 mM L-arginine. Aliquots were plated on L-arginine–containing plates for cfu determination. The dotted line represents the limit of detection. Data are representative of one of three independent experiments. Error bars show mean ± SD ($n = 3$).

Transcriptional Profiling and Flow Cytometry Analysis of Arginine-Deprived *Mtb* Reveal Envelope and Oxidative Stresses, ROS Accumulation, and DNA Fragmentation. We have demonstrated early up-regulation of the de novo arginine biosynthesis pathway by *Mtb* as an adaptive response to oxidative stress elevating the mycobactericidals INH or vitamin C. Furthermore, *argB* or *argF* deletion leads to sterilization of *Mtb* under arginine deprivation. Therefore, we conducted time-course transcriptomics and flow cytometry studies on arginine-deprived Δ*argB* and Δ*argF* mutants to investigate the mechanisms underlying their rapid death.

Transcriptomic microarrays analysis of arginine-deprived Δ*argB* (*SI Appendix*, Fig. S3 *A* and *B*) indicated a more than twofold increase in expression of genes for arginine biosynthesis (Fig. 2*A*), mycothiol, and the ergothioneine precursor histidine (*SI Appendix*, Fig. S3*C*). In contrast to the response of methionine-starved Δ*metA*, the only reported *Mtb* bactericidal amino acid auxotrophy, arginine-starved Δ*argB* at day 1, displayed induction of genes involved in cell-envelope stress and remodeling (including genes of the FAS II pathway); synthesis of mycolic acids, phospholipids, and glycans; and maintenance of membrane integrity as seen during INH treatment of *Mtb* (Fig. 2*A*) (19). *Mtb* genes involved in oxidative damage response, Fe-S cluster synthesis, as well as assembly (Fig. 2*B*) and Fe-S cluster-dependent essential enzymes (*SI Appendix*, Fig. S3*D*), were highly up-regulated (20). The bioenergetically less efficient microaerobic respiration pathway (*SI Appendix*, Fig. S3*E*) and the anaplerotic genes involved in an antioxidant defense to antibiotic stress (Fig. 2*C*) were also highly expressed (12, 21, 22). Increased ROS causes DNA damage, and there was a consequent up-regulation of genes involved in DNA repair (Fig. 2*B*) (3, 19). Increased expression of genes for arginine biosynthesis, antioxidant defense, and DNA repair genes was also observed in Δ*argF* (*SI Appendix*, Fig. S4 *A–C*), whereas the respiratory genes *nuoA–N* were down-regulated in both Δ*argB* and Δ*argF* (*SI Appendix*, Figs. S3*F* and S4*D*).

To extend our study of arginine-deprived Δ*argB*, we also performed RNA-Seq analysis following 4 and 48 h of arginine starvation. Consistent with the microarrays, genes involved in arginine biosynthesis were four- to sixfold up-regulated within 4 h of starvation. Significantly expressed genes (two- to fivefold) at 4 h included genes in cell-envelope remodeling (*lipX*, *pks4*) (23), sulfur import (Rv1463), heme binding at the cell surface for iron import PE22-PPE36 (24), and antioxidative response (*ahpC* and *ahpD*; Fig. 2*D*) (25). This was followed by a more than twofold enhanced expression of genes involved in the biosynthesis of thiols (mycothiol and the precursor of ergothioneine, histidine) and anaplerotic genes required for antioxidant defense against antibiotic stress at 48 h (*SI Appendix*, Fig. S3*G*). Genes involved in cell-envelope remodeling, antioxidant stress response, and DNA damage (*ung*) were also highly up-regulated at 48 h (Fig. 2 *E–G*). In contrast, at 4 and 48 h, *dosR*-regulated genes involved in hypoxia, Rv1404-regulated genes for a response against acid stress, and the *relA* regulon genes were three- to fourfold down-regulated (Fig. 2*D*) (25).

Our transcriptomics data on arginine-deprived Δ*argB* and Δ*argF* revealed signatures of oxidative stress, as seen in INH or vitamin C treatment of *Mtb* (9, 19). Therefore, we measured the accumulation of ROS in L-arginine–starved Δ*argB* and Δ*argF* by flow cytometry using fluorescent dihydroethidium dye and DNA damage using the terminal deoxynucleotidyl transferase-mediated dUTP-fluorescein nick-end labeling assay (TUNEL). The gating strategy used for both the assays is depicted in *SI Appendix*, Fig. S5. At day 1, we observed an approximately twofold increase in ROS in arginine-deprived Δ*argB* and Δ*argF* cultures compared with the arginine-supplemented cultures. In arginine-deprived Δ*argB*, from days 3–7, the ROS signal increased from approximately 6- to 20-fold over the nondeprived (Fig. 3*A*). In Δ*argF*, a slower increase of up to 12-fold at day 7 was observed (Fig. 3*A*). DNA damage in arginine-deprived cells correlated well with ROS accumulation and increased ∼25-fold (Δ*argB*) or ∼12-fold (Δ*argF*) compared with nondeprived cultures at day 7 (Fig. 3*B*).

To determine whether arginine deprivation enhances sensitivity to external ROS-mediated oxidative stress and DNA

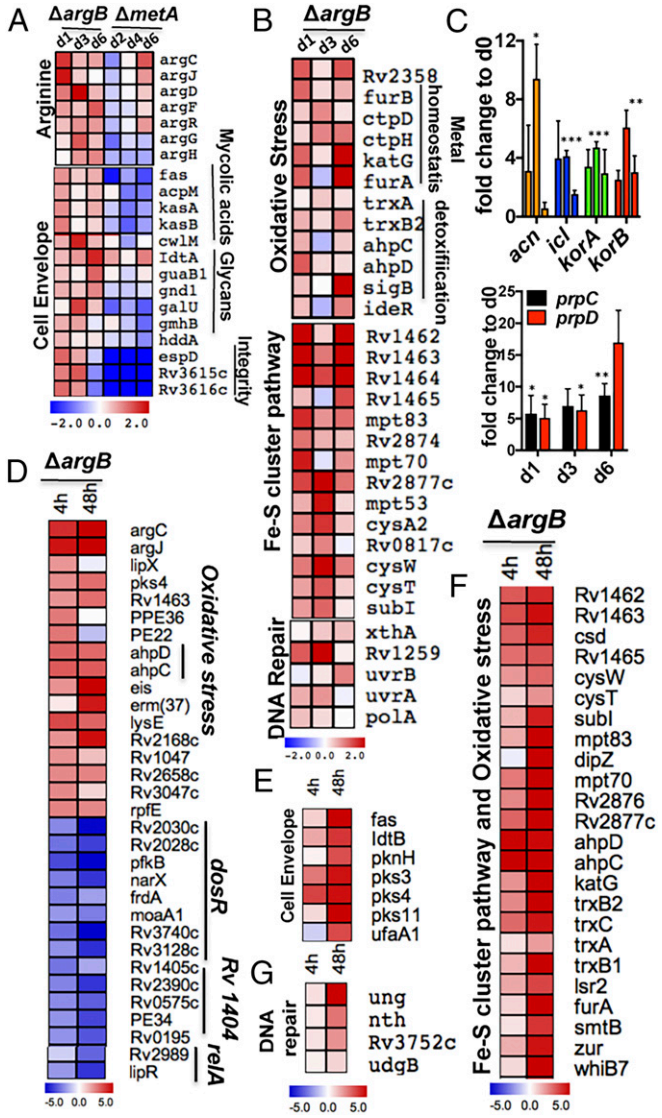

Fig. 2. Transcriptomic analysis of arginine-deprived *Mtb* Δ*argB* revealed signatures of cell-envelope stress and oxidative damage. To compare time-course changes in transcriptomic profiles of L-arginine–deprived H37Rv and Δ*argB*, RNA was isolated from samples harvested at 0, 1, 3, and 6 d for microarrays (*A*–*C*) and 0, 4, and 48 h for RNA-Seq (*D*–*G*). (*A*) Enhanced expression of genes involved in arginine biosynthesis and cell-envelope maintenance. (*B*) Up-regulation of genes associated with antioxidant defense, Fe-S cluster biosynthesis, and DNA repair. (*C*) Enhanced expression of anaplerotic genes (containing Fe-S) involved in antioxidant defense during antibiotic treatment (12). (*D*–*G*) RNA-Seq data of arginine-deprived *Mtb* Δ*argB*. (*D*) At 4 h of arginine starvation, genes involved in arginine biosynthesis, cell-envelope remodeling, antioxidative response, and heme and sulfur import were highly up-regulated. Conversely, *dosR*-, Rv1401-, and *relA*- regulated genes were down-regulated. (*E*–*G*) Up-regulation of genes involved in cell-envelope remodeling (*E*), Fe-S cluster biogenesis assembly and antioxidative defense (*F*), and DNA repair (*G*) at 48 h. Raw data for microarrays were deposited in the GEO database (accession no. GSE98821). All transcriptomic heat maps show log twofold changes. Mean with SD is plotted; error bars represent the SD of three independent biological replicates. $*P < 0.05$, $**P < 0.01$, $***P < 0.001$; two-tailed *t* test.

damage, we exposed day 1 arginine-starved Δ*argB* cells to 16 mM H_2O_2 for 4 h. An Δ*mshA* mutant deficient in mycothiol biosynthesis and hypersensitive to oxidative stress was used as a control (26). Within 4 h, we found approximately fivefold more ROS accumulation in Δ*argB* and Δ*mshA* than in H37Rv, although a decrease in ROS signal at later time points (days 2–3) was possibly due to nonviability of cells (*SI Appendix*, Fig. S6*A*). ROS production correlated well with increased DNA double-strand breaks. Within 4 h, H_2O_2 caused approximately twofold more DNA damage to Δ*argB* than to H37Rv (*SI Appendix*, Fig. S6*B*). To assess whether arginine-deprived *Mtb* is more sensitive to external ROS-mediated cell death, arginine-deprived Δ*argB* and Δ*argF* were treated at day 1 with 16 mM H_2O_2 for 4 h and plated to determine cfu on arginine-containing plates. The arginine-deprived mutants were highly sensitive and vulnerable to oxidative damage, as indicated by the approximately fivefold decreases in cfu within 4 h, but genetic complementation restored H_2O_2 sensitivity to H37Rv levels (*SI Appendix*, Fig. S6*C*).

To further test whether ROS has a role in the rapid killing of arginine-deprived Δ*argB*, cultures were starved for arginine in an hypoxic chamber containing 1% O_2 and 5% CO_2. The killing kinetics of arginine-starved Δ*argB* was reduced under hypoxic conditions (*SI Appendix*, Fig. S6*D*), suggesting a role for oxygen in the sterilization mechanism of arginine deprivation. Overall, our transcriptomics and flow cytometry data showed that arginine-deprived *Mtb* induces pleiotropic stress responses involving cell-envelope stress and ROS accumulation leading to DNA fragmentation and cell death.

Metabolomic Studies of Arginine-Deprived *Mtb* Show the Accumulation of Upstream Metabolites and Depletion of Antioxidant Thiols. To investigate the upstream molecular events underlying the ROS-mediated oxidative damage and cell death of arginine-deprived Δ*argB* and Δ*argF*, we conducted time-course metabolomics during arginine deprivation. Mutants and their complemented strains were grown in L-arginine–supplemented broth, washed, and then transferred to the arginine-free broth. Cells were harvested at days 0, 1, 3, and 6, and extracted metabolites were subjected to ultra-performance liquid chromatography mass spectrometry (UPLC-MS). Principal components analysis of *m*/*z* retention time pairs showed changes in the Δ*argB* metabolome over time (Fig. 4*A*), with substantial accumulation of the ArgB substrate *N*-acetyl-L-glutamate (~100-fold, Fig. 4*B*). The downstream metabolites, L-citrulline and L-arginine, decreased ~1,000-fold at day 1 and were later undetectable (Fig. 4*B*). At day 3, levels of ergothioneine and a compound with *m*/*z* 487.16 (consistent with mycothiol), which have roles in redox homeostasis (27), were decreased ~20-fold, whereas the secondary messenger cAMP accumulated by ~150-fold (Fig. 4*C*). In Δ*argF*, *N*-acetyl

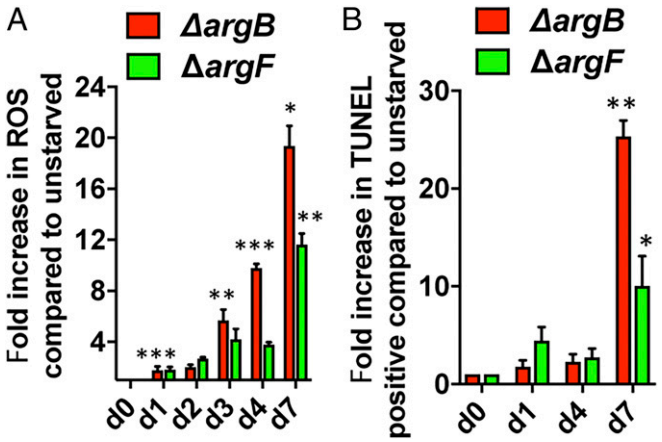

Fig. 3. Arginine deprivation leads to ROS accumulation and DNA damage. Δ*argB* and Δ*argF* were grown in L-arginine–supplemented 7H9 medium, washed, and transferred to L-arginine–deprived 7H9 medium. At the indicated time points, cell pellets were collected and stained with (*A*) dihydroethidium for ROS measurement or (*B*) TUNEL for measuring DNA double-stranded breaks using flow cytometry. Results were compared with nondeprived or untreated control samples. Mean ± SD is plotted ($n = 3$). $***P < 0.001$, $**P < 0.01$, $*P < 0.05$; Student's *t* test (two-tailed).

ornithine levels increased, and L-citrulline increased transiently before returning to initial levels while L-arginosuccinate and L-arginine were depleted below the detection limit after day 1 (*SI Appendix*, Fig. S4*E*). These results confirmed that arginine deprivation of *Mtb* leads to accumulation of upstream metabolite substrates of the deleted enzymes ArgB or ArgF and depletion of L-arginine, L-citrulline, and antioxidant thiols.

Arginine Deprivation Sterilizes *Mtb* in Immunocompetent and Immunocompromised Mice. Our previous results demonstrated that arginine deprivation leads to the rapid death of *Mtb* in vitro. Arginine concentration in mouse plasma is ~200 μM (28). Therefore, to determine whether *Mtb* can acquire arginine or pathway intermediates (ornithine and citrulline) in vivo, we tested the growth of the arginine auxotrophs Δ*argB* and Δ*argF* in immunocompetent C57BL/6 mice and in Severe Combined Immune-Deficient (SCID) mice. Following low-dose aerosol infection, both Δ*argB* and Δ*argF* were sterilized within 21 d in lungs of C57BL/6 mice (Fig. 5 *A* and *B*, *Left*) and were unable to disseminate to the spleen (Fig. 5 *A* and *B*, *Right*). Additionally, there was no sign of inflammation in the lungs at 4 wk postinfection (*SI Appendix*, Fig. S7*A*). In comparison, H37Rv and complemented strains (Δ*argB-c* and Δ*argF-c*) had increased burdens by 3 wk postinfection, with 10^4–10^6 cfu detected in lungs and spleen and gross pathology showing granulomatous lung disease (Fig. 5 *A* and *B* and *SI Appendix*, Fig. S7*A*). The rapid death phenotype of Δ*argB* and Δ*argF* was also observed in the lungs (Fig. 5*C*, *Upper Right*) and spleens (Fig. 5*C*, *Lower*) of aerosol-infected SCID mice, whereas H37Rv and complemented strains grew unimpeded, causing 100% mortality by 7–8 wk postinfection (Fig. 5*C*). There was no sign of disease pathology or acid-fast bacilli (AFB) in the lungs of SCID mice infected with Δ*argB* (Fig. 5*D* and *SI Appendix*, Fig. S7*B* and Table S4) or Δ*argF* (Fig. 5*E* and *SI Appendix*, Fig. S7*C* and Table S4). Conversely, mouse lungs infected with H37Rv or complemented *Mtb* strains exhibited severe lesions and tissue inflammatory infiltrates, primarily granulomas that obscured normal pulmonary architecture and that were often admixed with necrosis and associated with large numbers of AFB (Fig. 5 *D* and *E*, *Upper*; *SI Appendix*, Fig. S7 *B* and *C*, *Left*; and *SI Appendix*, Table S4).

Interestingly, Δ*argB* is so severely attenuated that even after i.v. infection with ~10^6 or 10^8 cfu, 100% of SCID mice were alive after 300 d, whereas those infected with H37Rv (10^8 cfu) died within 6 d (Fig. 5*F* and *SI Appendix*, Fig. S7*D*). Moreover, no mutant colonies or suppressors were recovered from lungs or spleens of SCID mice infected with Δ*argB* at 10^6 cfu (i.v.) even at 57 wk postinfection (*SI Appendix*, Fig. S7*D*). Together, these results establish that arginine deprivation causes rapid sterilization of *Mtb* cells in vivo without the emergence of any suppressor mutants and independently of the immune status of the host. These results suggest that *Mtb* is restricted to host niches where it cannot scavenge arginine or intermediates in the pathway, potentially due to

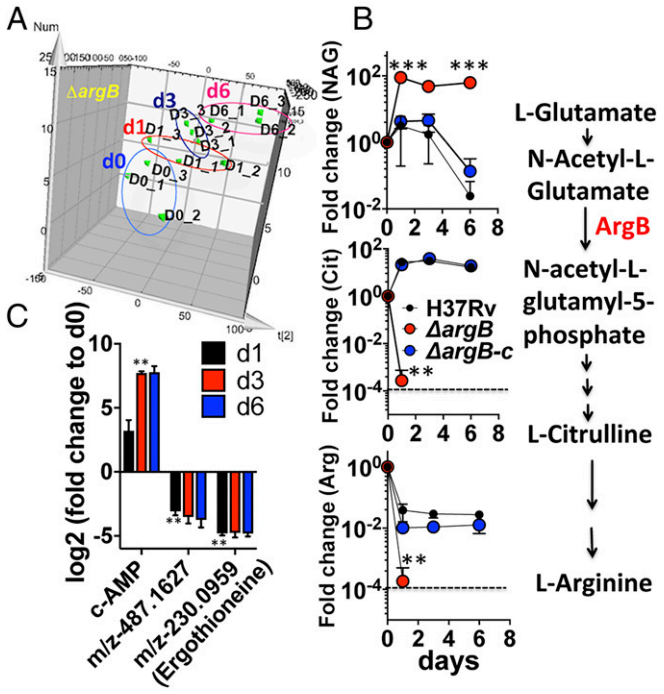

Fig. 4. Metabolomic analysis of arginine-deprived *Mtb* Δ*argB*. Time-course changes in metabolic profiles of H37Rv, Δ*argB*, and Δ*argB-c* were compared during 6 d of L-arginine deprivation. Samples were harvested at 0, 1, 3, and 6 d from three biologically independent replicates for extraction of metabolites. Aqueous-phase metabolites were measured by UPLC-MS, and fold changes in metabolite abundance were calculated relative to time 0. (*A*) Principal component analysis showed changes in the overall metabolomic profile of Δ*argB* over time during arginine deprivation. (*B*) Upstream metabolite *N*-acetyl glutamate (NAG), the substrate for ArgB, accumulated while the downstream metabolites L-citrulline and L-arginine were depleted. (*C*) Accumulation of cAMP and depletion of antioxidant thiols (ergothioneine and a compound with *m/z* 487.16, consistent with mycothiol). Error bars represent SD of three biological replicates. Dashed lines represent the limit of detection.

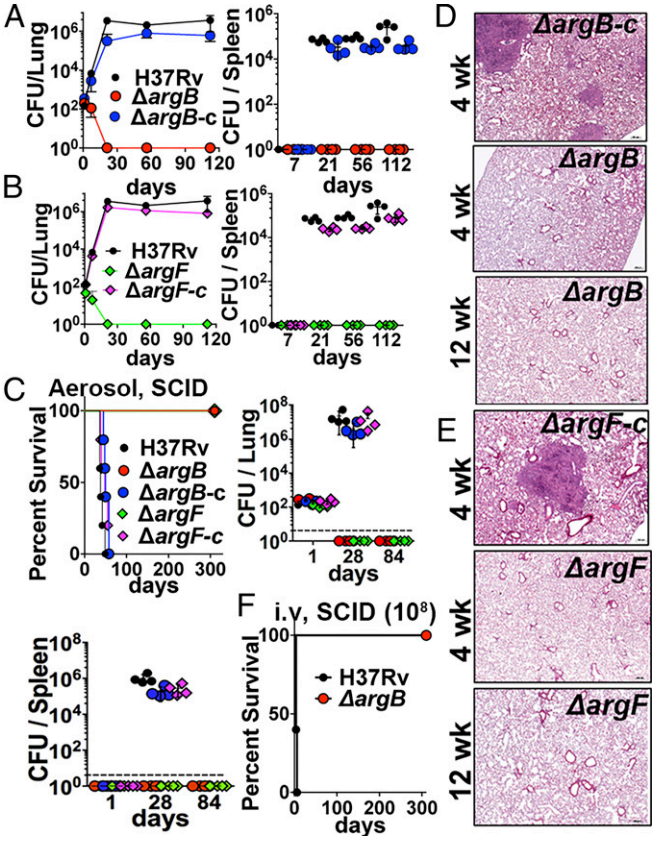

Fig. 5. *Mtb* arginine auxotrophic mutants are rapidly sterilized in immunocompetent (C57BL/6) and immunocompromised (SCID) mice. Mice were infected with low-dose aerosol (100 bacilli per animal) of strains Δ*argB*, Δ*argB-c* Δ*argF*, Δ*argF-c*, and H37Rv. Lung and spleen burdens were determined at days 1, 7, 21, 56, and 112 postinfection for C57BL/6 or at days 1, 28, and 84 postinfection for SCID. (*A* and *B*) The cfu in the lung (*Left*) and spleen (*Right*) of C57BL/6 mice. (*C*) Survival of SCID mice ($n = 6$) after low-dose aerosol infection (*Left*); cfu burden in lung and spleen (*Upper Right* and *Lower*, $n = 4$). (*D* and *E*) Lung histopathology of SCID mice. (*F*) Survival of SCID mice ($n = 6$) after high-dose (10^8 bacilli per animal) i.v. infection. One of two independent experiments is shown. Data are mean ± SD for $n = 4$ biological replicates. Dashed lines represent the limit of detection.

restricted availability or defective recruitment of arginine transport systems to the phagosome, thus leading to its rapid death.

Discussion

Shortening TB chemotherapy requires novel drugs that can rapidly sterilize *Mtb*. Our study provides compelling evidence that the arginine biosynthetic pathway is an attractive target for antitubercular drug development. Arginine deprivation leads to ROS accumulation, DNA damage, and rapid sterilization of *Mtb*.

ROS-mediated oxidative damage is a potent killing mechanism by bactericidal antibiotics for Gram-positive and Gram-negative bacteria, as well as *Mtb* (3–12). Our RNA-Seq data from *Mtb* treated with INH or vitamin C at 4 h indicated early up-regulation of de novo arginine biosynthesis. An increase in metabolites in the arginine biosynthesis pathway of *Mtb* at 24 h in monotherapy with the mycobactericidals INH, rifampicin, or streptomycin has been reported (12). Therefore, we investigated the role of the de novo arginine biosynthesis pathway in *Mtb*.

Arginine deprivation leads to a rapid sterilization of *Mtb* both in vitro and in vivo. Furthermore, no suppressor mutants were obtained when mice were challenged with Δ*argB* (10^8 cfu) or in three independent experiments on Middlebrook 7H9 media supplemented with oleic acid–albumin–dextrose–catalase OADC and glycerol up to 6 mo. While suppressors of complete gene deletions are very rare but could occur by biochemical bypass as has been observed for diaminopimelate auxotroph (29), these two sets of data suggest a multifactorial mechanism of death. Several potential mechanisms are possible such as futile cycling to generate precursors for arginine biosynthesis leading to enhanced ROS generation as observed in arginine-deprived cancer cells (14, 15). Our metabolomics studies showed an accumulation of *N*-acetyl glutamate and *N*-acetyl ornithine, an upstream metabolite substrate for ArgB or ArgF (Fig. 4 and *SI Appendix*, Fig. S4*E*). These intermediates are derived from L-glutamate, a precursor for L-arginine biosynthesis. This indicates that arginine-deprived *Mtb* is undergoing futile cycles to generate either L-glutamate from α-ketoglutarate or by glutamine. Both conditions are accompanied by increased flux into the tricarboxylic acid cycle and oxidative phosphorylation followed by ROS generation, DNA damage, and cell death. Another potential explanation is altered protein synthesis and secretion due to the indispensability of arginine for the twin-arginine transport (TAT) secretion signal motif "RR." TAT effectors are involved in respiration, nutrition uptake, and envelope maintenance (30–32). Defects in the TAT system are associated with cell death and envelope and oxidative stress susceptibility in many bacterial pathogens including *Mtb* (30, 31). Transcriptomics reveals that arginine-deprived *Mtb* exhibited up-regulation of signatures of envelope stress as seen during INH exposure (19) (Fig. 2*A*). Arginine is also the source of polyamines involved in scavenging ROS and protects membranes from lipid peroxidation in plants, bacteria, and parasites (16, 17, 33); similar mechanisms may be involved in *Mtb*. At day 3 of arginine deprivation, an ∼20-fold decrease was observed in the antioxidant thiols, ergothioneine, and a compound with an *m/z* 487.16, which corresponds to mycothiol (Fig. 4*C*). However, we have not detected the polyamines putrescine and agmatine in any sample possibly due to their lower abundance. We observed an ∼150-fold increase in accumulation of cAMP in arginine-deprived *Mtb* (Fig. 4*C*) in contrast to the observed depletion of cAMP in wild-type cells starved in PBS (34). The possibility of the accumulation of toxic metabolites or loss of an arginine-dependent essential metabolite contributing to killing was not ruled out, but we were unable to identify such metabolites. We propose a model in which futile cycles for generation of precursors for arginine biosynthesis, envelope stress, defects in protein synthesis and secretion, depleted thiols, or other undetermined factors initiate immediate and extreme oxidative stress, causing oxidative damage leading to multitargeted rapid *Mtb* death (*SI Appendix*, Fig. S8).

Much of *Mtb*'s success may stem from being self-sufficient as it has conserved biosynthesis pathways for most of the essential nutrients. While several *Mtb* amino acid auxotrophs are attenuated in vivo, only methionine deprivation has been reported to be bactericidal (35–40). In our study, high doses of Δ*argB* (10^6–10^8 cells) or Δ*argF* (10^6 cells) delivered via the i.v. route revealed that these arginine biosynthesis mutants were unable to replicate in SCID mice and were rapidly sterilized (Fig. 5). These results were somewhat unexpected, as *Mtb* has two arginine transporters (41) and serum concentrations of arginine are substantial (28). The inability of host-derived arginine to compensate for arginine auxotrophy reflects either inaccessibility of arginine in *Mtb* niches or inefficiency in expression, function, or translocation of import systems in vivo. Additionally, our results contrast with those using an *Mtb argF* mutant, which could acquire arginine, replicate in, and kill SCID mice (42). However, the above-mentioned study lacked an *argF*-complemented control strain, and the possibility of contamination with the parental or single cross-over strain during mouse infection cannot be ruled out.

This study underlines the critical sterilization role of the de novo arginine biosynthesis pathway for the survival of *Mtb* under arginine deprivation. This work suggests that the inhibitors against enzymes in this pathway have potential to sterilize *Mtb* and therefore can prevent or kill persistent populations. An absence of human homologs for many enzymes in the arginine biosynthetic pathway and lack of detection of arginine or its metabolites in NMR studies of lung granulomas of *Mtb*-infected guinea pigs (43) further reinforce the de novo arginine biosynthesis pathway as an excellent anti-TB drug target. These strains will provide a useful tool for screening novel inhibitors against enzymes in the arginine biosynthesis pathway using target-based approaches as whole-cell screening or new approaches as fragment-based drug discovery (44). Promising candidates that cocrystalize with enzymes in the de novo arginine biosynthesis pathway and inhibit its enzymatic activity could be tested for their potency and specificity in vitro and in vivo against *Mtb*. These strains are also a valuable tool to screen for compounds that act in synergy with arginine deprivation to enhance ROS-mediated *Mtb* cell death. Additionally, further insights into the common death mechanisms involved in arginine deprivation and other *Mtb* sterilization phenotypes will open avenues for drug screening to develop antibacterial strategies and interventions against *Mtb*.

Methods

See *SI Appendix, SI Methods*, for method details.

Bacterial Strains and Culture Conditions. All of the primers, plasmids, cosmids, and bacterial strains used in the study are listed in *SI Appendix*, Tables S1–S3. *Mtb* strains were grown at 37 °C in Middlebrook 7H9 liquid medium or 7H10 solid media supplemented with 10% OADC, 0.5% glycerol, and 0.05% tyloxapol. For *Mtb* strains bearing antibiotic cassettes, hygromycin (75 μg/mL) and/or kanamycin (20 μg/mL) were added wherever required. The L-arginine (1 mM) was added to liquid or solid media as described above. For the time-course starvation experiments, samples were grown in the presence of 1 mM L-arginine to 0.5 OD_{600}, washed with PBS tyloxapol (PBST), and switched to arginine-free medium. *Mtb* mutants were constructed by specialized transduction, unmarked and complemented as mentioned in *SI Appendix*.

RNA Isolation, Microarrays, and RNA-Seq. Samples were prepared in triplicate from cultures of H37Rv, Δ*argB*, and Δ*argF* for microarray analysis at days 0, 1, 3, and 6 and for RNA-Seq at 0, 4, and 48 h after starvation. RNA isolation, cDNA preparation, and microarray analysis were performed as described before (9). All of the data have been deposited at the National Center for Biotechnology Information (https://www.ncbi.nlm.nih.gov/geo/) under accession number GSE98821. For RNA-seq, libraries were prepared and checked for quality on a 2100 Bioanalyzer. Sequencing of 75-bp paired-end reads was performed on the Illumina HiSEq. 4000 platform followed by differential expression analyses, normalization of raw counts, and generation of heat maps. Details can be found in *SI Appendix*.

Flow Cytometry-Based ROS Detection and DNA Fragmentation Assays. *Mtb* strains were grown in 7H9 media with or without L-arginine to OD_{600} ∼ 0.8. Cultures were pelleted and washed five times with PBST and diluted to OD_{600} ∼ 0.2 in fresh media with or without L-arginine or H_2O_2. Aliquots were

removed at indicated time points, and cells were washed twice in PBS and stained with dihydroethidium for 30 min at 37 °C. Cells were analyzed immediately on a BD FACS Calibur (BD Biosciences) with the following instrument settings: forward scatter (FSC), EO2 log gain; side scatter, 550V log; fluorescence (FL1), 674V log; fluorescence (FL2), 628V log and threshold set on SSC (236V). For each sample, 10,000 events were acquired. The analysis was performed by using unlabeled and untreated/treated cells as negative controls and gating intact cells. DNA strand breaks in *Mtb* strains undergoing starvation or H_2O_2 treatment were measured by TUNEL assay using the in situ cell death detection kit (Roche). Additional details are given in *SI Appendix*.

Metabolite Extraction and Mass Spectroscopy. Bacterial strains were grown in L-arginine media to OD_{600} (~0.5–0.6), washed, and transferred to starvation media. The 5-mL samples (OD_{600} of 0.5) were quickly quenched in 10 mL methanol at −20 °C. Samples were centrifuged at 3,300 × *g*/10 min/−9 °C. Cell pellets were suspended in 1 mL extraction solvent [40% acetonitrile (vol/vol), 40% methanol (vol/vol), and 20% water (vol/vol)] and transferred to screw-cap tubes containing silica beads. Cells were lysed and processed, and samples collected at various time points (days 0, 1, 3, and 6) were analyzed using an Acquity UPLC system (Waters) coupled with a Synapt G2 quadrupole-time-of-flight hybrid mass spectrometer. Method details, metabolite abundances, retention time, and *m/z* values can be found in *SI Appendix*, *SI Methods* and Dataset S1.

Animal Experiments and Pathology. All animal protocols used were approved by the Animal Use and Care Committee of the Albert Einstein College of Medicine (Bronx, NY). The 6- to 8-wk-old C57BL/6 and SCID mice (Jackson Laboratories) were infected with *Mtb* and various mutants via the aerosol route using a 1×10^7 cfu/mL mycobacterial suspension in PBST and 0.004% antifoam. Infection yielded ~100 bacilli per lung. To determine bacterial burden, four mice were killed at various mentioned time points. Lungs and spleens were harvested and plated to determine cfu. For SCID i.v. infections, strains grown to midlog phase were washed and injected via tail vein (10^6 or 10^8 cfu/mouse). Lung tissues were fixed in 10% (vol/vol) formalin for 48–72 h, followed by paraffin-embedded sectioning and H&E or acid-fast staining. Five or six mice per group were kept for survival experiments. All mice infected with *Mtb* were maintained under appropriate conditions in an animal biosafety level 3 laboratory. All experiments were repeated to confirm the reproducibility.

ACKNOWLEDGMENTS. We thank Regy Lukose, Annie Zhi Dai and Laura Cole for technical support, Core Facilities at Albert Einstein College of Medicine; Dr. Amanda Beck for histopathology; Dr. Paras Jain and Dr. Lydia Tesfa (Grant P30CA013330) for flow cytometry. We thank students Lara Kleinfelter, Karen Giraldo and Humira Ferdush for their help in different aspects of paper. This work was supported by a Human Challenge grant from the Bill and Melinda Gates Foundation, a grant from the National Institutes of Health (R01AI026170) and Wellcome Trust Grant 098051.

1. Koul A, Arnoult E, Lounis N, Guillemont J, Andries K (2011) The challenge of new drug discovery for tuberculosis. *Nature* 469:483–490.
2. Levin-Reisman I, et al. (2017) Antibiotic tolerance facilitates the evolution of resistance. *Science* 355:826–830.
3. Imlay JA, Chin SM, Linn S (1988) Toxic DNA damage by hydrogen peroxide through the Fenton reaction in vivo and in vitro. *Science* 240:640–642.
4. Kohanski MA, Dwyer DJ, Hayete B, Lawrence CA, Collins JJ (2007) A common mechanism of cellular death induced by bactericidal antibiotics. *Cell* 130:797–810.
5. Dwyer DJ, et al. (2014) Antibiotics induce redox-related physiological alterations as part of their lethality. *Proc Natl Acad Sci USA* 111:E2100–E2109.
6. Belenky P, et al. (2015) Bactericidal antibiotics induce toxic metabolic perturbations that lead to cellular damage. *Cell Rep* 13:968–980.
7. Rasouly A, Nudler E (2018) Antibiotic killing through oxidized nucleotides. *Proc Natl Acad Sci USA* 115:1967–1969.
8. Dhandayuthapani S, Zhang Y, Mudd MH, Deretic V (1996) Oxidative stress response and its role in sensitivity to isoniazid in mycobacteria: Characterization and inducibility of ahpC by peroxides in Mycobacterium smegmatis and lack of expression in M. aurum and M. tuberculosis. *J Bacteriol* 178:3641–3649.
9. Vilchèze C, Hartman T, Weinrick B, Jacobs WR, Jr (2013) *Mycobacterium tuberculosis* is extraordinarily sensitive to killing by a vitamin C-induced Fenton reaction. *Nat Commun* 4:1881–1891.
10. Vilchèze C, et al. (2017) Enhanced respiration prevents drug tolerance and drug resistance in *Mycobacterium tuberculosis*. *Proc Natl Acad Sci USA* 114:4495–4500.
11. Fan XY, et al. (2018) Oxidation of dCTP contributes to antibiotic lethality in stationary-phase mycobacteria. *Proc Natl Acad Sci USA* 115:2210–2215.
12. Nandakumar M, Nathan C, Rhee KY (2014) Isocitrate lyase mediates broad antibiotic tolerance in *Mycobacterium tuberculosis*. *Nat Commun* 5:4306.
13. Middlebrook G, Cohn ML, Schaefer WB (1954) Studies on isoniazid and tubercle bacilli. III. The isolation, drug-susceptibility, and catalase-testing of tubercle bacilli from isoniazid-treated patients. *Am Rev Tuberc* 70:852–872.
14. Qiu F, et al. (2014) Arginine starvation impairs mitochondrial respiratory function in ASS1-deficient breast cancer cells. *Sci Signal* 7:ra31.
15. Kremer JC, et al. (2017) Arginine deprivation inhibits the Warburg effect and upregulates glutamine anaplerosis and serine biosynthesis in ASS1-deficient cancers. *Cell Rep* 18:991–1004.
16. El-Halfawy OM, Valvano MA (2014) Putrescine reduces antibiotic-induced oxidative stress as a mechanism of modulation of antibiotic resistance in *Burkholderia cenocepacia*. *Antimicrob Agents Chemother* 58:4162–4171.
17. Mandal A, et al. (2016) Deprivation of L-arginine induces oxidative stress mediated apoptosis in *Leishmania donovani* promastigotes: Contribution of the polyamine pathway. *PLoS Negl Trop Dis* 10:e0004373.
18. Sassetti CM, Boyd DH, Rubin EJ (2003) Genes required for mycobacterial growth defined by high density mutagenesis. *Mol Microbiol* 48:77–84.
19. Boshoff HI, et al. (2004) The transcriptional responses of *Mycobacterium tuberculosis* to inhibitors of metabolism: Novel insights into drug mechanisms of action. *J Biol Chem* 279:40174–40184.
20. Huet G, Daffé M, Saves I (2005) Identification of the *Mycobacterium tuberculosis* SUF machinery as the exclusive mycobacterial system of [Fe-S] cluster assembly: Evidence for its implication in the pathogen's survival. *J Bacteriol* 187:6137–6146.
21. Voskuil MI, Bartek IL, Visconti K, Schoolnik GK (2011) The response of *Mycobacterium tuberculosis* to reactive oxygen and nitrogen species. *Front Microbiol* 2:105.
22. Matsoso LG, et al. (2005) Function of the cytochrome bc1-aa3 branch of the respiratory network in mycobacteria and network adaptation occurring in response to its disruption. *J Bacteriol* 187:6300–6308.
23. Dubey VS, Sirakova TD, Kolattukudy PE (2002) Disruption of msl3 abolishes the synthesis of mycolipanoic and mycolipenic acids required for polyacyltrehalose synthesis in Mycobacterium tuberculosis H37Rv and causes cell aggregation. *Mol Microbiol* 45:1451–1459.
24. Mitra A, Speer A, Lin K, Ehrt S, Niederweis M (2017) PPE surface proteins are required for heme utilization by Mycobacterium tuberculosis. *MBio* 8:1–14.
25. Cumming BM, et al. (2014) The physiology and genetics of oxidative stress in mycobacteria. *Microbiol Spectr* 2:1–22.
26. Vilchèze C, et al. (2008) Mycothiol biosynthesis is essential for ethionamide susceptibility in *Mycobacterium tuberculosis*. *Mol Microbiol* 69:1316–1329.
27. Saini V, et al. (2016) Ergothioneine maintains redox and bioenergetic homeostasis essential for drug susceptibility and virulence of *Mycobacterium tuberculosis*. *Cell Rep* 14:572–585.
28. Gobert AP, et al. (2000) L-Arginine availability modulates local nitric oxide production and parasite killing in experimental trypanosomiasis. *Infect Immun* 68:4653–4657.
29. Consaul SA, Jacobs WR, Jr, Pavelka MS, Jr (2003) Extragenic suppression of the requirement for diaminopimelate in diaminopimelate auxotrophs of Mycobacterium smegmatis. *FEMS Microbiol Lett* 225:131–135.
30. Sargent F, Berks BC, Palmer T (2002) Assembly of membrane-bound respiratory complexes by the Tat protein-transport system. *Arch Microbiol* 178:77–84.
31. McDonough JA, et al. (2008) Identification of functional Tat signal sequences in *Mycobacterium tuberculosis* proteins. *J Bacteriol* 190:6428–6438.
32. Oertel D, Schmitz S, Freudl R (2015) A TatABC-type Tat translocase is required for unimpaired aerobic growth of *Corynebacterium glutamicum* ATCC13032. *PLoS One* 10:e0123413.
33. Saha J, et al. (2015) Polyamines as redox homeostasis regulators during salt stress in plants. *Front Environ Sci* 3:21.
34. Kahramanoglou C, et al. (2014) Genomic mapping of cAMP receptor protein (CRP Mt) in *Mycobacterium tuberculosis*: Relation to transcriptional start sites and the role of CRPMt as a transcription factor. *Nucleic Acids Res* 42:8320–8329.
35. Zhang YJ, Rubin EJ (2013) Feast or famine: The host-pathogen battle over amino acids. *Cell Microbiol* 15:1079–1087.
36. Gouzy A, Poquet Y, Neyrolles O (2014) Nitrogen metabolism in *Mycobacterium tuberculosis* physiology and virulence. *Nat Rev Microbiol* 12:729–737.
37. Hondalus MK, et al. (2000) Attenuation of and protection induced by a leucine auxotroph of *Mycobacterium tuberculosis*. *Infect Immun* 68:2888–2898.
38. Lee S, et al. (2006) Protection elicited by two glutamine auxotrophs of *Mycobacterium tuberculosis* and in vivo growth phenotypes of the four unique glutamine synthetase mutants in a murine model. *Infect Immun* 74:6491–6495.
39. Smith DA, Parish T, Stoker NG, Bancroft GJ (2001) Characterization of auxotrophic mutants of *Mycobacterium tuberculosis* and their potential as vaccine candidates. *Infect Immun* 69:1142–1150.
40. Berney M, et al. (2015) Essential roles of methionine and S-adenosylmethionine in the autarkic lifestyle of *Mycobacterium tuberculosis*. *Proc Natl Acad Sci USA* 112:10008–10013.
41. Peteroy-Kelly MA, Venketaraman V, Talaue M, Seth A, Connell ND (2003) Modulation of J774.1 macrophage L-arginine metabolism by intracellular *Mycobacterium bovis* BCG. *Infect Immun* 71:1011–1015.
42. Gordhan BG, et al. (2002) Construction and phenotypic characterization of an auxotrophic mutant of *Mycobacterium tuberculosis* defective in L-arginine biosynthesis. *Infect Immun* 70:3080–3084.
43. Somashekar BS, et al. (2011) Metabolic profiling of lung granuloma in *Mycobacterium tuberculosis* infected guinea pigs: Ex vivo 1H magic angle spinning NMR studies. *J Proteome Res* 10:4186–4195.
44. Mendes V, Blundell TL (2017) Targeting tuberculosis using structure-guided fragment-based drug design. *Drug Discov Today* 22:546–554.